Regulation of developing myelin sheath elongation by oligodendrocyte calcium transients *in vivo*

Anna M. Krasnow[1], Marc C. Ford[1], Leonardo E. Valdivia[2+],

Stephen W. Wilson[2] & David Attwell[1]

[1]Department of Neuroscience, Physiology & Pharmacology

[2]Department of Cell and Developmental Biology

University College London,

Gower Street, London, WC1E 6BT, UK

Before publication: Address correspondence to David Attwell, d.attwell@ucl.ac.uk

After publication: Address correspondence to

Anna Krasnow, anna.krasnow.12@ucl.ac.uk or David Attwell, d.attwell@ucl.ac.uk

[+]Current address: Center for Integrative Biology, Facultad de Ciencias, Universidad Mayor, Chile.

Supported by a Wellcome Trust 4 year PhD studentship (099691/Z/12/Z) to AMK, an EU Marie Curie Fellowship (623714) to MCF, Wellcome Trust Investigator Awards to DA (099222/Z/12/Z) and SW (104682/Z/14/Z), and a MRC programme grant (MR/L003775/1) to SW and G. Gestri.

We thank I.L. Arancibia-Carcamo, I. Bianco, E. Dreosti, V. Kyrargyri and W.T. Sherlock for comments, and Fish Facility personnel for care of fish.

How action potentials regulate myelination by oligodendrocytes is uncertain. We show that neuronal activity raises $[Ca^{2+}]_i$ in developing oligodendrocytes *in vivo*, and that myelin sheath elongation is promoted by a high frequency of $[Ca^{2+}]_i$ transients and prevented by $[Ca^{2+}]_i$-buffering. Sheath elongation occurs ~1 hour after $[Ca^{2+}]_i$ elevation. Sheath shortening is associated with a low frequency of $[Ca^{2+}]_i$ transients but with longer duration $[Ca^{2+}]_i$ bursts. Thus, $[Ca^{2+}]_i$ controls myelin sheath development.

Neuronal action potentials may regulate myelination, both during development[1-3] and during white matter plasticity in adulthood[4,5]. Possible mediators of neuronal activity include exocytosis[6-8] of glutamate[9,10] or GABA[11] at synapses between unmyelinated axons and oligodendrocyte precursor cells[12], or release of growth factors[10,13]. Within developing oligodendrocytes these agents may alter the concentration of calcium[14].

To investigate whether $[Ca^{2+}]_i$ regulates myelination *in vivo*, we studied developing oligodendrocytes in the spinal cords of zebrafish (immobilised in agarose at 3 days post-fertilisation). Their spinal cord was imaged employing membrane-associated fluorescent proteins encoded by *tg(sox10:mRFP)* or *tg(mbp:mCherry)* transgenes to reveal the structure of developing oligodendrocytes, and *tg(sox10:GCaMP6s)* transgene to monitor $[Ca^{2+}]_i$. In some animals CRISPR/Cas9-mediated somatic silencing of the *tg(sox10:mRFP)* transgene in most cells enabled observation of single cells developing. We classified cells into 3 developmental stages. Pre-myelinating oligodendrocytes (pre-OLs, Fig. 1a) showed many processes, none of which had made a sheath. Since *tg(sox10:mRFP)* can be expressed in interneurons, these cells' identity was confirmed by observing them until they formed myelin sheaths. Early oligodendrocytes (early-OLs, Fig. 1b) had started to make sheaths. Oligodendrocytes (OLs, Fig. 1c) had initiated formation of all the sheaths that would be produced (as confirmed by subsequent observation), placing them past the 5 hour window[15] of sheath initiation, although a small fraction of sheaths could still shorten and disappear in these cells[15].

Cells at all stages exhibited $[Ca^{2+}]_i$ transients (quantified as in the Online Methods) in their processes and somata (Fig. 1d-f; interactions between $[Ca^{2+}]_i$ transients in different locations are presented in Supp. Fig. 1). The overall transient rate declined with development and was similar (Fig. 1g) in each process (where they may regulate local cytoskeletal events and/or protein and lipid synthesis) and in somata (where they may regulate gene expression). Because there are many processes per cell (10.3±0.6 analysed in pre-OLs, 11.9±0.6 in early-OLs and 6.9±0.6 in OLs), most transients occurred in processes rather than somata. However, $[Ca^{2+}]_i$ transients were >2-fold longer in the somata (Fig. 1h). The amplitude of transients (assessed as $\Delta F/F$, where F is GCaMP6s fluorescence) declined in processes with development, and was smaller in somata than in processes throughout development (Fig. 1i).

To determine whether neuronal activity generated oligodendrocyte $[Ca^{2+}]_i$ transients, we stimulated action potentials electrically or blocked them by injecting TTX (or extracellular solution, sham) into the hindbrain, from where it entered the spinal cord (Fig. 2a-c). Stimulated action potentials were detected as extracellular field potentials, which were stable during sham injections but abolished by TTX (Fig. 2c). Averaging responses to 10 second 50 Hz stimulation trains revealed that stimulation significantly increased $[Ca^{2+}]_i$, both in processes that had not yet made a sheath ("Non-sheath", part of pre-OLs or early-OLs: Fig. 2d) and in sheaths of processes that were already myelinating ("Sheath", part of early-OLs or OLs, Fig. 2e). The $[Ca^{2+}]_i$ transient amplitude was larger in Non-sheath than in Sheath processes (Fig. 2d-e). Stimulation increased the frequency of $[Ca^{2+}]_i$ elevations (Fig. 2f-g), but by less than the 0.6/min (1/100 sec) increase expected if every stimulation train evoked a $[Ca^{2+}]_i$ rise. Neuronal stimulation also evoked $[Ca^{2+}]_i$ rises in somata of cells with processes that had not yet made a sheath, but not in somata of cells that already had a sheath-forming process (Fig. 2h-k) implying that at this later developmental stage neuronal activity releases factors that raise $[Ca^{2+}]_i$ in developing sheaths but not in somata.

Injecting extracellular solution had no effect on ongoing $[Ca^{2+}]_i$ transients in the processes and somata of oligodendrocyte-lineage cells, but TTX injection roughly halved the

transient rate in processes (Fig. 2l-m). TTX produced a similar reduction of transient rate in somata of cells with non-sheath processes (Fig. 2n-o). Thus, approximately half of the $[Ca^{2+}]_i$ transients in developing oligodendrocytes are driven by axonal action potentials, but the remainder occur independently of action potentials.

To determine whether myelin sheath $[Ca^{2+}]_i$ transients regulate sheath growth, we imaged growing sheaths in OLs for 10.5 minutes every hour for 5 hours (Fig. 3a-b). This allowed measurement of the $[Ca^{2+}]_i$ transient frequency without excessive fluorophore bleaching or phototoxicity while imaging structural changes over an extended period. Over 5 hours, the lengths of myelin sheaths increased (44% of 68 sheaths studied), decreased (26%), showed no change (24%), or increased then decreased (6%) (Fig. 3c-e). Plotting the total change of sheath length against the mean $[Ca^{2+}]_i$ transient rate in that sheath over 5 hours revealed that sheath elongation correlated strongly with $[Ca^{2+}]_i$ transient rate (Fig. 3f; regression slope is different from zero, $p=10^{-11}$). However, for a $[Ca^{2+}]_i$ transient rate lower than ~1/30 mins, sheath retraction occurred. Thus, a threshold rate of $[Ca^{2+}]$ transients may be needed to maintain sheath length at this developmental stage.

Similar plots showed that sheath elongation also correlated weakly but significantly (Supp. Fig. 2a-c) with sheath $[Ca^{2+}]_i$ transient amplitude, duration and area ($\int[\Delta F/F].dt$), but not with the somatic $[Ca^{2+}]_i$ transient rate (Supp. Fig. 2d). Thus, sheath development is correlated with local $[Ca^{2+}]_i$ changes but not with somatic changes that might alter global gene expression. To assess the temporal relationship between $[Ca^{2+}]_i$ elevations and sheath length, we selected sheaths which showed no growth for at least one hour (e.g. red lines in Fig. 3c), and aligned their time course of sheath elongation and $[Ca^{2+}]_i$ transient rate at the onset of growth (Supp. Fig. 2e). Plotting sheath growth per hour against mean $[Ca^{2+}]_i$ transient rate (assessed as the average of the rates in imaging periods bracketing that hour) suggested that an increase in transient rate triggers sheath elongation after ~1 hour (Fig. 3g).

To demonstrate that the $[Ca^{2+}]_i$ transients, including those evoked by neuronal activity (Fig. 2), mechanistically drive sheath elongation (rather than merely being correlated

with elongation), we first modulated neuronal activity and hence the $[Ca^{2+}]_i$ transient rate, either increasing neuronal activity with stimulation or decreasing it with TTX (Fig. 3h). Stimulation increased sheath elongation by 60% (Fig. 3i), while TTX reduced elongation by 43% (Fig. 3j). Second, we manipulated the $[Ca^{2+}]_i$ changes occurring within growing myelin sheaths, by briefly whole-cell patch-clamping developing oligodendrocytes to introduce into them solutions of low (1 mM EGTA) or high (30 mM BAPTA) $[Ca^{2+}]$ buffering power (with the same free $[Ca^{2+}]_i$: ~63 nM, see Online Methods). Sheaths dialysed with the weak buffer continued to elongate over 3 hours, while those dialysed with the strong buffer on average shortened (significantly different, $p=2x10^{-4}$, Fig. 3k). Thus, myelin sheath elongation is driven by $[Ca^{2+}]_i$ transients, including those evoked by neuronal activity.

In addition to the temporally-isolated $[Ca^{2+}]_i$ transients associated with sheath lengthening, we observed a longer type of $[Ca^{2+}]_i$ event ('bursts', inset to Fig. 3l) exhibiting repeated rises and falls of $[Ca^{2+}]_i$ (duration 87.5±15.8 sec [mean±SEM, n=7]; mean $\Delta F/F$ 0.52±0.09. These were rare but, strikingly, occurred only in sheaths that were shortening (or transitioning from growing to shortening). Consequently, isolated transients and bursts are inversely correlated in their association with sheath behaviour (Fig. 3l). On average $[Ca^{2+}]_i$ bursts contributed only 7.8±2.8% of the Ca^{2+} entry (calculated as $\int[\Delta F/F].dt$) in all sheaths, but this was 0% in lengthening sheaths, and 75.6±2.2% in shortening sheaths with bursts. Dialysis with the BAPTA internal is expected to reduce the $[Ca^{2+}]_i$ during these events, so the fact that sheaths shortened in this condition (Fig. 3k) suggests that a BAPTA-induced reduction of magnitude of the brief $[Ca^{2+}]_i$ transients dominates the effect on sheath length, or that the large Ca^{2+} entry occurring during bursts overwhelms the BAPTA buffer.

Our data show that, like astrocytes[16], developing oligodendrocytes *in vivo* exhibit spatially-restricted $[Ca^{2+}]_i$ elevations. At early developmental stages these can occur simultaneously in many cell processes (possibly due to simultaneous neuronal input), but as myelination proceeds they become independent in different growing sheaths (Fig. 1, Supp. Fig. 1). Approximately half of these transients are evoked by action potentials, as they are

blocked by TTX and their rate is increased by electrical stimulation (Fig. 2). They may be generated by synaptic input from unmyelinated axons[12], although this is downregulated as oligodendrocytes mature[17]. The remainder of the transients appear to be generated spontaneously, perhaps by TRPA1 channels[16] in oligodendrocyte sheaths[18]. Conceivably, since $[Ca^{2+}]_i$ transients promote sheath growth, these spontaneous and activity-driven transients may underlie the activity-independent and activity-dependent forms of myelination reported previously[10].

Lengthening of the myelin sheath is driven by the rate of $[Ca^{2+}]_i$ transients occurring (Fig. 3) and, below a certain rate, sheaths shorten, so a minimum $[Ca^{2+}]_i$ transient rate may be needed to maintain sheath length. However, long duration $[Ca^{2+}]_i$ bursts imparting a high calcium load are also associated with shortening. These results suggest that modest $[Ca^{2+}]_i$ elevations trigger sheath elongation, while very low or excessively large rises lead to sheath shortening. The $[Ca^{2+}]_i$ transients presumably control proteins regulating cytoskeletal growth and myelin assembly. A likely effector producing sheath elongation is the PI3K/Akt/mTOR pathway, which is Ca^{2+}-activated[19] and promotes myelin growth when activated in oligodendrocytes[20]. Although our observations are in developing oligodendrocytes, it will be intriguing to determine whether the same is true in established sheaths in adult animals, given that myelin plasticity is increasingly invoked as a mechanism for learning[4,5], and during remyelination following stroke, spinal cord injury or multiple sclerosis.

References

1. Demerens, C. et al., *Proc. Natl. Acad. Sci. U.S.A.* **93**, 9887-9892 (1996).

2. Stevens, B., Porta, S., Haak, L.L., Gallo, V. & Fields, R.D. *Neuron* **36**, 855-868 (2002).

3. Gibson, E.M. et al. *Science* **344**, 1252304 (2014).

4. Bengtsson, S.L. et al. *Nat. Neurosci.* **8**, 1148–1150 (2005).

5. Sampaio-Baptista, C. et al. *J. Neurosci.* **33**, 19499-19503 (2013).

6. Mensch, S. et al., *Nat. Neurosci.* **18**, 628-630 (2015).

7. Hines, J.H., Ravanelli, A.M., Schwindt, R., Scott, E.K. & Appel, B. *Nat. Neurosci.* **18**, 683-689 (2015).

8. Koudelka, S. et al., *Curr. Biol.* **26**, 1447-1455 (2016).

9. Gallo, V., et al. *J. Neurosci.* **16**, 2659-2670 (1996).

10. Lundgaard, I., et al. *PLoS Biol.* **11**, e1001743 (2013).

11. Hamilton, N.B. et al., *Glia* **65**, 309-321 (2017).

12. Bergles, D.E., Roberts, J.D., Somogyi, P. & Jahr, C.E. *Nature* **405**, 187-191 (2000).

13. Ozaki, M., Itoh, K., Miyakawa, Y., Kishida, H., Hashikawa, T. *J. Neurochem.* **91**, 176–188 (2004).

14. Sun, W., Matthews, E.A., Nicolas, V., Schoch, S. & Dietrich, D. *Elife* **5**, e16262 (2016).

15. Czopka, T., ffrench-Constant, C. & Lyons, D.A. *Dev. Cell* **25**, 599-609 (2013).

16. Shigetomi, E., Tong, X., Kwan, K.Y., Corey, D.P. & Khakh, B.S. *Nat. Neurosci.* **15**, 70-80 (2011).

17. Kukley, M., Nishiyama, A. & Dietrich, D. *J. Neurosci.* **30**, 8320-8331 (2010).

18. Hamilton, N.B., Kolodziejczyk, K., Kougioumtzidou, E. & Attwell, D. *Nature* **529**, 523-527 (2016)..

19. Zonouzi, M., Renzi, M., Farrant, M. & Cull-Candy, S.G. *Nat. Neurosci.* **14**, 1430-1438 (2011).

20. Goebbels, S. et al. *J. Neurosci.* **30**, 8953-8964 (2010).

Figure Legends

Figure 1. Calcium transient properties change during oligodendrocyte development.

(**a-c**) Oligodendrocyte morphology at different developmental stages (3 cells from different CRISPR/Cas9-injected *tg(sox10:mRFP)* fish for each stage): (**a**) pre-OLs, before sheaths have been initiated; (**b**) early-OLs, when some sheaths have been initiated; (**c**) OLs, when all sheaths have been initiated. (**d-f**) Specimen $[Ca^{2+}]_i$ traces for 3 developmental stages showing: (top) sequentially-recorded traces for the somata of 6 cells, and (bottom) simultaneously-recorded traces in different processes of a single cell of each class. A $[Ca^{2+}]_i$ rise (red triangle) occurs simultaneously in 4 processes in d. (**g-i**) Rate, duration and amplitude of the transients at the 3 developmental stages (n=10 pre-OLs, 8 early-OLs and 8 OLs from 5, 6 and 6 animals respectively). P values are from 2-tailed tests: one-way ANOVA followed by Holm-Bonferroni-corrected t-tests in g for 'all processes', and h and i for 'processes'; Kruskal-Wallis followed by Dunn's test in g for 'per process' and 'somata', and in h and i for 'somata'; two-way ANOVA followed by Holm-Sidak in h and i for 'somata' vs. 'processes'. Data are mean±SEM.

Figure 2. Neuronal activity evokes half the calcium transients in developing oligodendrocytes.

(**a**) Stimulating spinal cord rostral to the imaged area, and recording evoked activity caudally. In some experiments, TTX or Sham injections were into the hindbrain; 15 mins was allowed for diffusion to the imaged area. (**b**) Stimulation: 50 Hz pulses for 10 seconds, repeated 7 times every 100 seconds. (**c**) Field potential recording (at 1 Hz) before and after TTX (9 animals) or Sham solution (8 animals) injection showed abolition by TTX but not Sham. Calcium imaging was performed before and after the injection (red vertical lines). (**d-e**) $[Ca^{2+}]_i$ traces (mean±SEM in grey) averaged over 7 periods without or with stimulation (red rectangles) in (**d**) 18 Non-sheath forming or (**e**) 45 Sheath forming processes. (**f-g**) Mean±SEM (points are individual processes) rate of $[Ca^{2+}]_i$ transients without and with stimulation in (**f**) Non-sheath forming or (**g**) Sheath forming processes. (**h-k**) As for d-g but

for somata (9 each for j and k). Experiments in d-k were from 5 animals. (**l-m**) Rate of $[Ca^{2+}]_i$ transients before and after Sham or TTX injections in (**l**) Non-sheath forming (27 and 32 processes for Sham and TTX respectively) or (**m**) Sheath forming processes (59 and 61 processes for Sham and TTX). (**n-o**) As for l-m but for somata (18 and 19 somata for Sham and TTX in n; 25 and 27 somata for Sham and TTX in o). Number of animals for l-o was as in c. Statistical tests (2-tailed) used: Wilcoxon signed rank test in f, g, j; paired t-test in k; repeated measures ANOVA followed by Holm-Sidak for l, m-o. Data are mean±SEM.

Figure 3. Myelin sheath elongation correlates with calcium transient rate.

(**a**) Schematic of calcium imaging protocol. (**b**) Specimen images (5 hours apart) of *tg(mbp: mCherry-CAAX)* (hotter colours indicate more fluorescence, left scale) in developing oligodendrocytes. Red, blue and white arrows indicate sheaths that became longer, shorter or did not change length, respectively, over 5 hours. Experiments were repeated six times with similar results. (**c-e**) Sheath behaviour over time in 3 cells to illustrate diversity of behaviour. Pie charts show percentage of sheaths growing (red; 75% in c, 42.9% d, 37.5% e), growing then shortening (purple; 25% c, 14.3% d), shortening (blue; 14.3% d, 62.5% e), and not changing length (black; 28.6% d). (**f**) Change of sheath length over 5 hours as a function of mean $[Ca^{2+}]_i$ transient rate (see Online Methods) in 68 sheaths. (**g**) Increase of sheath length per hour and $[Ca^{2+}]_i$ transient rate in 14 sheaths which were of constant length for at least 1 hour before lengthening started (at t=0). Data are mean±SEM. (**h**) Protocols for experiments in i (top) and j (bottom). Large lines: structural stack acquisition; small red lines: stimulation. (**i-j**) Sheath growth over 5 hours in (**i**) 78 sheaths in 5 sham-stimulated fish and 71 sheaths in 5 stimulated fish, and (**j**) 99 sheaths in 6 sham-injected fish and 93 sheaths in 6 TTX-injected fish (box and whisker plots show median, 25th and 75th centiles, and most extreme data values). (**k**) Sheath growth over 3 hours for oligodendrocytes briefly whole-cell clamped with internal solution containing 1 mM EGTA (Ctrl, 24 sheaths from 6 fish) or 30 mM BAPTA (21 sheaths from 5 fish). (**l**) Percentage of sheaths with different growth behaviour (G, growth; 0, no change, G->S, growing then shortening, S, shortening)

exhibiting >1 Ca^{2+} transients in the 63 mins imaged over 5 hours (black, left axis) or showing $[Ca^{2+}]_i$ bursts (red, right axis). Insets show specimen transients and bursts (scale bars 1 min and $\Delta F/F=1$). Different growth states are associated with significantly different numbers of transients (Chi-squared $p=10^{-5}$, n=68 sheaths from 6 animals) and bursts ($p=9x10^{-4}$). Because $[Ca^{2+}]_i$ was only sampled for 10.5 mins per hour, and bursts are rare, it is possible that all (rather than 33% of) shortening sheaths experience $[Ca^{2+}]_i$ bursts. Two-tailed statistical tests used: linear regression t-statistic in f; Mann-Whitney in i, j; unpaired t-test in k; Chi-squared test in l.

Online Methods

Animals

The following transgenic zebrafish lines were used: *tg(sox10:mRFP)*^{vu234Tg} (ref. 21, kindly provided by D. Lyons, Edinburgh) and two lines generated in house, *tg(mbp:mCherry-CAAX)*^{u4011} and *tg(sox10:GCaMP6s)*^{u4016}. The red-fluorescing *tg(sox10:mRFP)* and *tg(mbp:mCherry)* lines were used to visualise oligodendrocyte structure early and late in development, respectively, and the green-fluorescing *tg(sox10:GCaMP6s)* line was used to detect $[Ca^{2+}]_i$ changes. To visualise the morphology of single cells, CRISPR/Cas9 was used to achieve mosaic expression of the mRFP fluorophore (see below). All experiments were performed in the non-pigmented nacre background (*mitfa*$^{w2/w2}$). Embryos were collected by natural spawning, and raised at 28.5°C in fish water. Animal procedures were carried out in accordance with the guidelines of the UK Animals (Scientific Procedures) Act 1986 and European Directive 2010/63/EU. Animals were randomly assigned to different treatments.

Plasmid construction

Constructs were generated with Gateway cloning technology using the clones p5E-*mbp*[22], p5E-*sox10* (generated by excising the *sox10* promoter from[23] p-4.9*sox10:egfp* and ligating into p5E-MCS), pME-GCaMP6s (generated in a BP reaction from pGP-CMV-GCaMP6s [Addgene]) and components of the Tol2kit[24]: p3E-polyA, pME-mCherryCAAX, pDestTol2pA2 and pDestTol2CG2. Vectors were recombined using LR clonase II Plus (Invitrogen). Gateway BP clonase II was used to generate pME-GCaMP6s.

Generation of transgenic zebrafish lines

Fertilized eggs were injected with 1 nl of solution containing 25 ng/µl of plasmid DNA and 100 ng/µl of transposase mRNA. Injected embryos were grown to adulthood and F1 offspring were screened by phenotype (expression of fluorescent protein in the appropriate cells) to identify F0 founders.

CRISPR mosaics

We used CRISPR/Cas9 genome editing to perform somatic inactivation (in most cells) of the mRFP transgene in a stable transgenic fish line *tg(sox10:mRFP)*^{vu234Tg} in order

to allow visualisation of single developing oligodendrocytes. Guide RNA design was performed[25] with CHOPCHOP (https://chopchop.rc.fas.harvard.edu/) using the mRFP sequence as input. One to 16 cell stage embryos were injected with 150 pg Cas9 and 30 pg mRFP gRNA (with target sequence GGCGAGGGCCGCCCCTACG), and embryos were selected for imaging based on their mosaic expression of the fluorescent marker.

Live imaging

At 3 days post fertilisation (dpf) larvae were mounted in 1% LMP agarose (Sigma, made up in fish water) in 0.5 mg/ml mivacurium chloride (LKT labs, a neuromuscular blocker used to prevent movement) and imaged at 28-29^{o}C with a Zeiss LSM780 two-photon/confocal microscope. A confocal stack was taken in an area between segments 8 and 14 of the spinal cord, to record the morphology of developing oligodendrocytes (*sox10:mRFP* or *mbp:mCherry-CAAX*, excited at 561 nm). In calcium imaging experiments GCaMP6s was two-photon excited at 940 nm, with an intensity at the preparation of 11 mW and a pixel dwell time of 2.55 μsec, using a W Plan-Apochromat x20 objective with NA=1.0. Stacks of 5 planes, 2 μm apart, were acquired every 3.5 s for 10.5 min (180 stacks). In Fig. 1 calcium imaging was performed once for each field of view, in Fig. 2 twice for each field of view (control and stimulation, or control and TTX or sham injection) and in Figs. 3a-g and 3l six times (every hour for 5 hours, see Fig. 3a). The spatial resolution provided by 2-photon imaging did not allow us to define whether sheath $[Ca^{2+}]_i$ transients occur between the lamellae of the developing sheath or in the cytoplasmic tongues extending along the sheath. Lengths of myelin sheaths were measured in a maximum intensity projection of the GCaMP6s images, i.e. averaged over the 10.5 mins of calcium imaging. This procedure was shown (in control experiments) to give the same measured length as when measuring the *tg(sox10:RFP)* or *tg(mbp:mCherry)* images. It is not possible to tell from our images the extent to which the sheaths have started compacting at the stage imaged (compaction is a gradual process, starting in the outer wraps, that occurs only as the sheath develops[26]). This does not affect our conclusions in any way, since the great majority of the sheaths we are

studying are destined to become compacted[26,15] (and only a small fraction of sheaths are removed[15]).

Image analysis

Regions of interest (ROIs) were drawn for each non-sheath process (the terminal ~2-5 μm portion of a non-myelinating process) or sheath. The GECIquant 1.0 plugin[27] for ImageJ was used to create time profiles of ΔF/F, where F is the fluorescence of GCaMP6. In MATLAB, for each ROI we calculated a locally time-smoothed baseline (using uk.mathworks.com/matlabcentral/fileexchange/24916-baseline-fit with the piecewise cubic Hermite interpolating polynomial uk.mathworks.com/help/matlab/ref/pchip.html) with a smoothing time of 60 frames for cell processes and 120 frames for somata (which have longer $[Ca^{2+}]_i$ transients). Then, we defined $[Ca^{2+}]_i$ elevations of potential interest, using a detection threshold set to 2.25 x standard deviation of the first 100 points in the trace with ΔF/F<0.75 (to exclude contributions of $[Ca^{2+}]_i$ transients to the baseline) for the processes and set to 1 x standard deviation of the first 100 points in the trace with ΔF/F<0.2 for the somata (somata data were subsequently smoothed by averaging each 2 adjacent points). These $[Ca^{2+}]_i$ elevations were then further selected or rejected in the supra-threshold graph using a minimal area criterion ($\int [\Delta F/F]\, dt$ > 0.275 frames for processes and > 0.24 frames for somata). Results of these analyses, which were carried out in MATLAB, were manually checked against the original GCaMP6s recordings to exclude false positives (resulting from increases in background activity, or activity in other cell processes). In Fig. 1g transient rate is shown for 'Somata' (averaged over cells), 'Per process' (calculated by obtaining the mean rate per process for each cell and then calculating the mean±SEM by averaging over all cells), and for 'All processes' (calculated by averaging over all cells the product of [mean rate per process for each cell].[number of processes on the cell]).

Duration of transients or bursts (Fig. 1h, Supp. Fig. 2b) was taken as the time for which they were above the detection threshold. Amplitude (Fig. 1i, Supp. Fig. 2a) was taken as the magnitude of ΔF/F at the peak of the response relative to the time-smoothed baseline.

Transient area (Supp. Fig. 2c) was taken as the sum of: (i) the area of the transient above the threshold, and (ii) its 'base', taken as the duration of the transient multiplied by the threshold value (which is the area of the transient below the threshold). Rarely observed $[Ca^{2+}]_i$ bursts, defined as periods of raised $[Ca^{2+}]_i$, with frequently alternating sub- and suprathreshold values of $\Delta F/F$, with the suprathreshold events constituting at least 55% of the frames, and with an overall duration greater than 40 sec, were excluded from the analysis of transients for Fig. 3f, and analysed separately for Fig. 3l. Burst area was calculated as the sum of the areas of each supra-threshold component of the burst plus its 'base'. Mean burst amplitude was calculated as the burst area divided by its duration. The average rate (Fig. 3f), amplitude, duration and area (Supp. Fig. 2a-c) of calcium transients were calculated using the flanking calcium recordings to obtain an average for each hour and then taking the sum of those and dividing it by the total duration of the experiment.

Electrical stimulation and pharmacology

A stimulation electrode (glass capillary filled with 1M NaCl) was inserted in the rostral spinal cord. For recording field potentials, a similar electrode (tip resistance 15–35 MΩ inside the spinal cord) was placed in the caudal spinal cord. Stimuli (single pulses applied at 1 Hz, or 50 Hz stimulus trains of 10 s duration) were generated with a GRASS S88 stimulator triggered with Clampex software (Axon Instruments, Molecular Devices). For these experiments the fish was surrounded by fish extracellular solution (134 mM NaCl, 10 mM HEPES, 10 mM glucose, 2.9 mM KCl, 2.1 $CaCl_2$, and 1.2 mM $MgCl_2$) rather than fish water, to allow better current flow from the stimulation electrode to the ground electrode. Field potentials (for TTX experiments measured in voltage-clamp mode as currents) were recorded using an Axon Instruments MultiClamp 700B amplifier. Data were digitized at 10 kHz using an Axon Instruments Digidata 1440 (Molecular Devices). Stimulation strength was set to 15–100 V (depending on the electrode resistance) to reliably evoke field potentials. When imaging calcium with and without stimulation (Fig. 2b, d-k), the periods of stimulation and no stimulation (control) were alternated, and $[Ca^{2+}]_i$ transient rate was measured in a

40s time window which included the 10s stimulation and the 30s post-stimulation periods (equivalent time windows were analysed in the control experiments where no stimulation was applied). To block action potentials in the spinal cord, 2 nl of fish extracellular solution containing 2 μM TTX was pressure injected into the brain using a Picospritzer III (Parker). Injections were calibrated to deliver 0.5 μl per pressure pulse (4 pulses were used for 2 μl). For control injections (sham), the same volume of extracellular solution lacking TTX was injected (no blinding of experimenters to the identity of the injected solution was used for these experiments). Movement of TTX from the injection site to the spinal cord (to inhibit action potentials) took <1 min, and we waited 15 mins to ensure that it reached the imaging site (Fig. 2c). Experiments in Fig. 3i had the stimulation and recording electrodes inserted but not the injection pipette; experiments in Fig. 3j had injection pipette inserted but not the stimulation and recording electrodes.

Whole-cell patch-clamp loading of calcium buffer into oligodendrocytes *in vivo*

After immobilization using 0.50–0.55 mg/ml mivacurium chloride dissolved in fish external solution, fish were pinned through the notochord to a sylgard-coated recording chamber using fine tungsten needles. The skin was removed using a tungsten tool and fine tweezers, and the muscles aspirated using a suction electrode. Oligodendrocytes were identified by mCherry expression and patch-clamped using 15-18 MΩ patch pipettes. Directly after establishing the whole-cell configuration (with cells voltage-clamped at -55mV), 4-5 brief “zaps” (25 μs, 1 volt pulse, applied from the Multiclamp 700B amplifier) were applied to load the cell with the internal solution (monitored by the spread of the Alexa Fluor 647 dye included in the internal solution). Directly after zapping, the patch pipette was retracted carefully to allow the membrane to reseal (monitored in voltage-clamp mode). The tissue was allowed to relax for approximately 15 minutes before imaging. Image stacks (image size 70.7 μm x 41.4 μm, pixel size 0.14 μm, z step size 1 μm) of the patch-clamp loaded oligodendrocytes were taken every hour for a period of 3 hours.

The control (low calcium buffer) internal solution contained (in mM) 125 potassium gluconate, 2 NaCl, 0.2 $CaCl_2$, 10 HEPES, 1 EGTA, 2 $MgCl_2$, 2 Mg-ATP, 0.5 Na_2-GTP, 10 Na_2-phosphocreatine and 0.1 Alexa Fluor 647, with pH set to 7.1 using KOH. The high calcium buffering power internal solution contained BAPTA (tetrapotassium salt) and was similar, but with the $CaCl_2$ and EGTA replaced with (in mM) 7 $CaCl_2$ and 30 BAPTA, and with osmolarity differences compensated by lowering the potassium gluconate concentration. The solution contained (in mM) 63 K-gluconate, 2 NaCl, 7 $CaCl_2$, 10 HEPES, 30 K_4-BAPTA, 2 $MgCl_2$, 2 Mg-ATP, 0.5 Na_2-GTP, 10 Na_2-phosphocreatine and 0.1 Alexa Fluor 647, with pH set to 7.1 using KOH. The free $[Ca^{2+}]_i$ was ~63 nM in both internal solutions, calculated using MaxChelator (http://maxchelator.stanford.edu/webmaxc/webmaxcS.htm) with the temperature set to 28°C and ionic strength set to 140 mM.

The experimenter was blinded as to whether the pipette contained the low or high calcium buffer solution.

Statistics

Data are shown as mean±SEM, with individual data points superimposed. N numbers used for statistics were of cell processes, sheaths or somata, as appropriate. Normality of data was verified using the D'Agostino & Pearson omnibus test and equality of variance tested using the F-statistic. Normally distributed data were analysed using ANOVA and post-hoc t-tests, or paired t-tests, as appropriate. For t-tests, data were compared to interleaved controls using a homoscedastic, two-sided Student's t-test (equal variance), except where the variances of the data were unequal, when a heteroscedastic, two-sided Student's t-test was used. Data were corrected for multiple comparisons within figure panels using a procedure equivalent to the Holm-Bonferroni method (for N comparisons, the most significant p value is multiplied by N, the 2nd most significant by N-1, the 3rd most significant by N-2, etc.; corrected p values are significant if they are less than 0.05). Non-normally distributed data were analysed with (two-tailed) Kruskal-Wallis tests followed by Dunn's multiple comparison tests, or Wilcoxon tests, as appropriate (in GraphPad Prism). Differences between processes and somata in Fig. 1h-i were analysed with a two-way

ANOVA followed by Holm-Sidak's multiple comparison test. Data in Fig. 2l-o were analysed with a two-way repeated measures ANOVA followed by Holm-Sidak's multiple comparison test. Comparisons of the slopes of linear regressions with a slope of zero were performed using the t-statistic for the regression. Comparison of the numbers of $[Ca^{2+}]_i$ transients or bursts in different process categories was done with Chi-squared tests. Further details of statistical tests are available in Supplementary Table 1.

An estimate of the sample size needed for a typical experiment is as follows. For a control response of 100%, a typical response standard deviation of 40%, a response at a different developmental stage of 30% (70% less), a power of 80% and $p<0.05$, 7 cell processes are needed (http://www.biomath.info/power/ttest.htm) in each of the two groups. The exact numbers depend on the effect size and standard error of the data.

Data availability

The data that support the findings of this study are available from the corresponding author upon reasonable request. The MATLAB code used can be obtained from https://github.com/AttwellLab/MyelinCalcium. A Life Sciences Reporting Summary is available.

Materials

TTX citrate was obtained from Abcam and mivacurium chloride from LKT labs. Other chemicals were from Sigma.

Data and Code Availability

Available from the corresponding author upon request.

Author contributions

The work was conceived by AMK and DA. AMK generated the transgenic lines with help from LEV. AMK devised and performed imaging and some electrophysiological experiments with advice from LEV and SWW. MCF devised methods for electrical stimulation and whole-cell patch clamping and performed electrophysiology, whole-cell patch clamping experiments and some other imaging experiments. AMK, MCF and DA analysed the data. SWW and DA provided zebrafish, imaging and electrophysiology resources. DA and AMK wrote the manuscript, with input from all authors.

Supplementary References

21. Kirby, B.B. et al. *Nat. Neurosci.* **9**, 1506-1511 (2006).

22. Almeida, R.G., Czopka, T., ffrench-Constant, C. & Lyons, D.A. *Development* **138**, 4443-4450 (2011).

23. Carney, T.J. et al. *Development* **133**, 4619-4630 (2006).

24. Kwan, K.M. et al. *Dev. Dyn.* **236**, 3088-3099 (2007).

25. Montague, T.G., Cruz, J.M., Gagnon, J.A., Church, G.M. & Valen, E. *Nucleic Acids Res.* **42**, W401-407 (2014).

26. Snaidero, N. et al. *Cell* **18**, 314-323 (2014).

27. Srinivasan, R. et al. *Nat. Neurosci.* **18**, 708-717 (2015).

Supplementary Figure Legends

Supplementary Figure 1. Synchronicity of $[Ca^{2+}]_i$ transients in different cell regions. (**a-c**) Charts: Fraction of time (Probability) that the number of processes on the abscissa (*N*) had a simultaneous $[Ca^{2+}]_i$ elevation, in (**a**) pre-OLs, (**b**) early-OLs and (**c**) OLs from 5, 6 and 6 animals respectively (mean values, shown as horizontal lines with SEM bars, that are below all visible individual data points reflect some data points being zero and hence not plotted on the logarithmic scale charts). Inset tables: Observed distribution of probability as in main graphs, and predicted distribution calculated as follows. If the probability of a single observed process having a high $[Ca^{2+}]_i$ is denoted p_1 (this was derived experimentally for each process and averaged over all the processes of each individual cell), and there are *N* processes, the probability of *k* processes exhibiting calcium transients simultaneously is: $p(k) = \frac{N! p_1^k (1-p_1)^{N-k}}{k!(N-k)!}$. These are the predicted values in the inset tables, when averaged over all cells. The observed values for the fraction of time that 2 or more processes simultaneously showed a high $[Ca^{2+}]_i$ were greater than predicted for pre-OLs and early-OLs, implying cooperativity of transient generation between processes or propagation of transients from one process into another, but not for OLs (see 2-sided Chi-squared p values for inset tables). (**d-f**) Probabilities of *N* (abscissa) processes having high $[Ca^{2+}]_i$ simultaneously and having the soma $[Ca^{2+}]_i$ low (black bars) or high (i.e. during a soma $[Ca^{2+}]_i$ transient, grey bars), for each of the 3 classes of cell. (**g-i**) Cumulative probability distributions for the data in d-f, with p values from Kolmogorov-Smirnov tests comparing the distributions for each cell class. When the soma $[Ca^{2+}]_i$ was high in early-OLs, there was a larger probability for 1 or more processes to have an elevated $[Ca^{2+}]_i$, than was the case when the soma $[Ca^{2+}]_i$ was low. Soma transients occurred with a probability of 0.10, 0.08 and 0.02 for pre-OLs, early-OLs and OLs, respectively, and so the majority of $[Ca^{2+}]_i$ transients in processes occurred when soma $[Ca^{2+}]_i$ was low. In OLs in particular, processes only showed $[Ca^{2+}]_i$ elevations when the soma $[Ca^{2+}]_i$ was low, and the data in panel c imply that $[Ca^{2+}]_i$ transients in different myelin sheaths are independent of each other. (**j-l**)

Probability of the soma $[Ca^{2+}]_i$ being high when the number of processes on the abscissa simultaneously exhibited high $[Ca^{2+}]_i$ for each of the 3 classes of cell. For pre-OLs the probability of the soma $[Ca^{2+}]_i$ being high is increased when more processes have a simultaneously high $[Ca^{2+}]_i$ ($p=0.0024$, ANOVA) indicating that gene expression might be controlled by somatic $[Ca^{2+}]_i$ elevations triggered by simultaneous activity-evoked transients in several processes on the same developing oligodendrocyte. For early-OLs the increase of probability with number of processes simultaneously exhibiting high $[Ca^{2+}]_i$ did not reach significance ($p=0.86$, Kruskal-Wallis test). For OLs, the soma $[Ca^{2+}]_i$ was never high when process $[Ca^{2+}]_i$ was high. All data are mean±SEM.

Supplementary Figure 2. Dependence of sheath elongation on $[Ca^{2+}]_i$ properties.

(a**-c**) Change of sheath length (in 68 sheaths from 6 animals) correlates significantly with sheath $[Ca^{2+}]_i$ transient (**a**) duration, (**b**) amplitude and (**c**) area (∫[ΔF/F] dt). (**d**) Change of sheath length does not correlate significantly with soma $[Ca^{2+}]_i$ transient rate (in 54 sheath-soma pairs from 6 animals). (**e**) Increase of sheath length and $[Ca^{2+}]_i$ transient rate in 14 lengthening sheaths which were of constant length for at least 1 hour before lengthening started, with data aligned at t=0 at the start of growth. $[Ca^{2+}]_i$ transients precede sheath growth by ~1 hour. Data are mean±SEM.

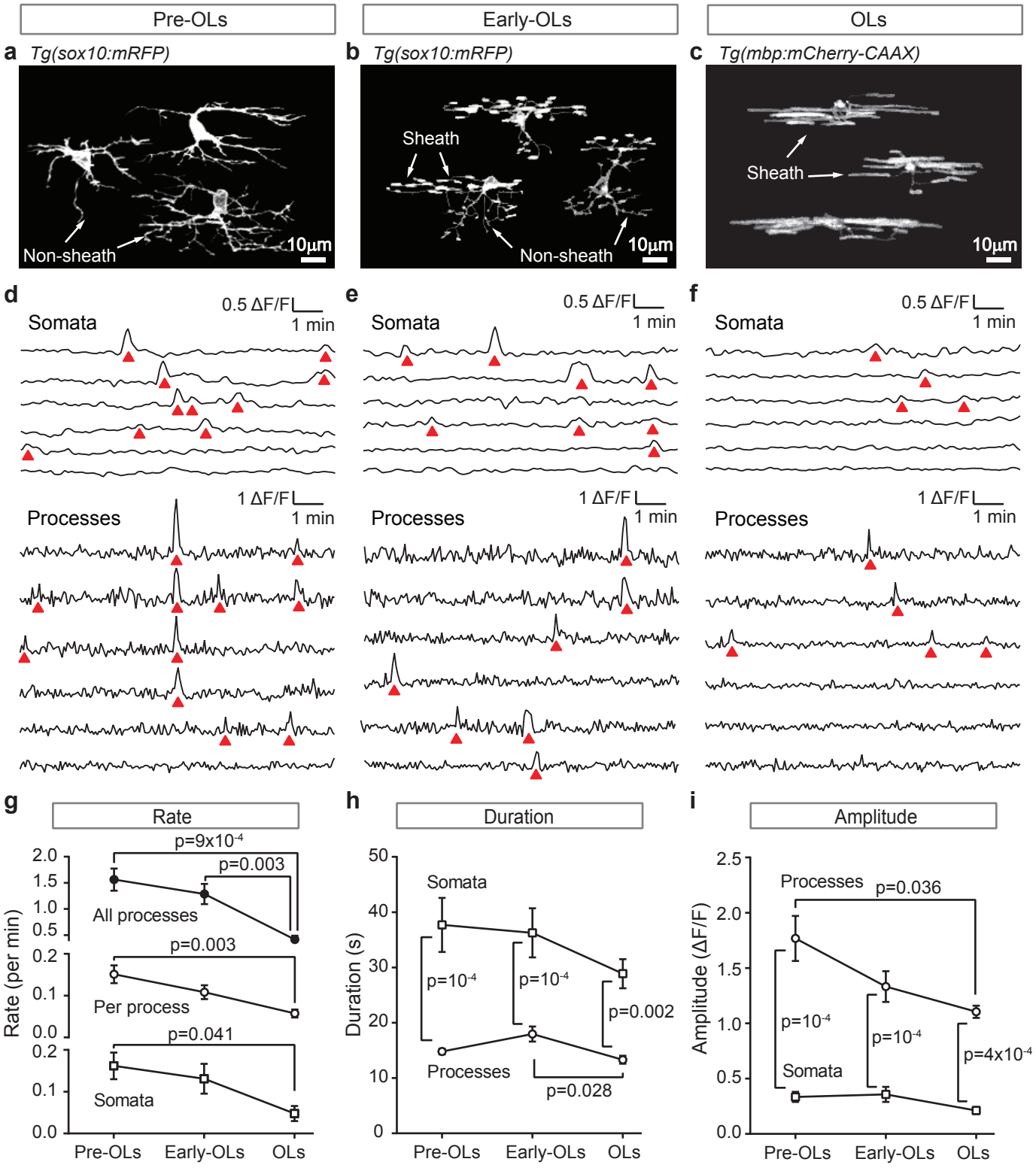
Pre-OLs
Early-OLs
OLs
a Tg(sox10:mRFP)
b Tg(sox10:mRFP)
c Tg(mbp:mCherry-CAAX)
Sheath
Non-sheath
10µm
Sheath
Non-sheath
10µm
Sheath
10µm
d
e
f
Somata
0.5 ΔF/F
1 min
Processes
1 ΔF/F
1 min
g
Rate
Rate (per min)
p=9x10-4
p=0.003
All processes
p=0.003
Per process
p=0.041
Somata
Pre-OLs
Early-OLs
OLs
h
Duration
Duration (s)
Somata
p=10-4
p=10-4
p=0.002
Processes
p=0.028
i
Amplitude
Amplitude (ΔF/F)
Processes
p=0.036
p=10-4
p=10-4
p=4x10-4
Somata

Fig. 1

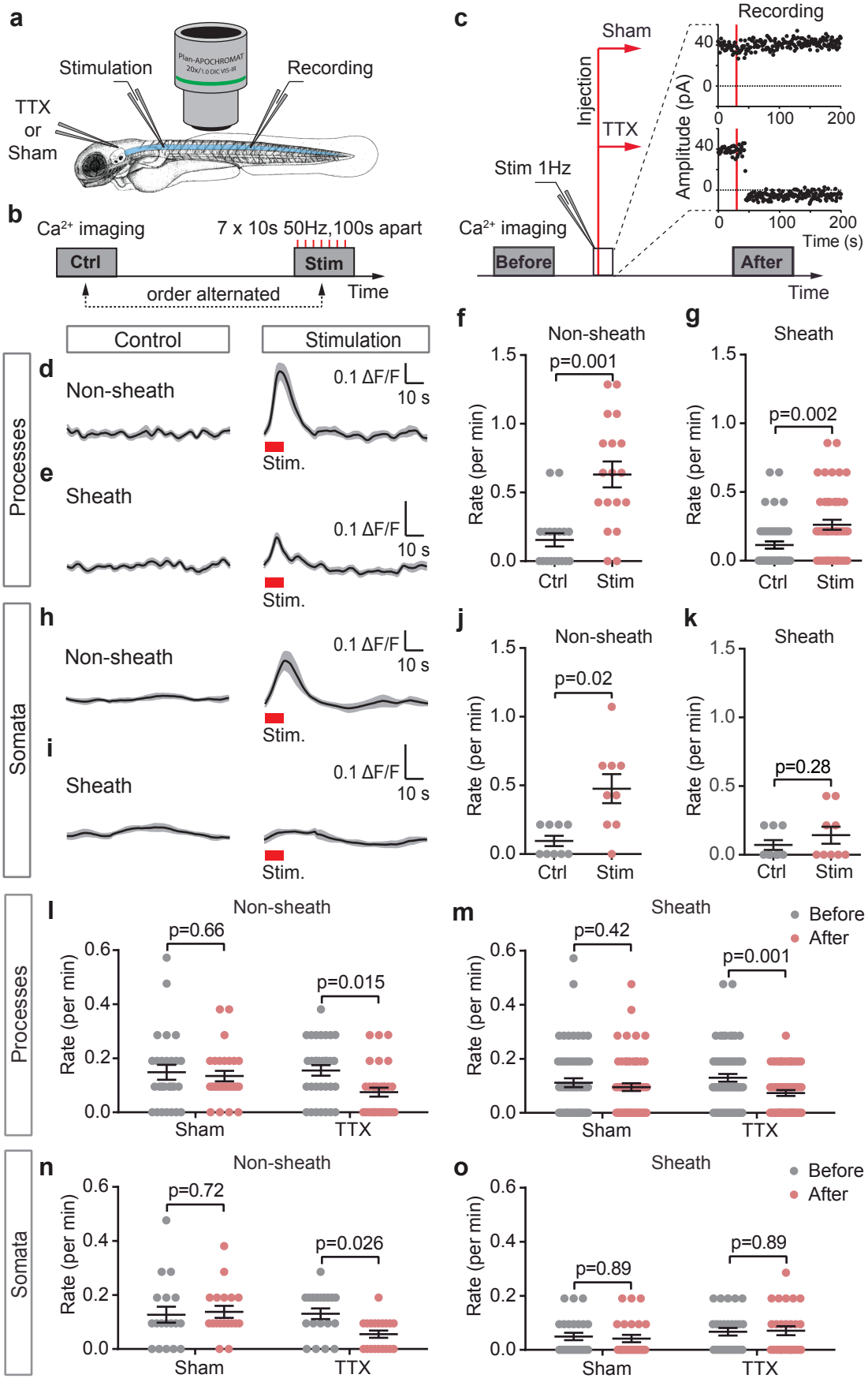
a
Stimulation
Recording
TTX
or
Sham
b
Ca2+ imaging
7 x 10s 50Hz,100s apart
Ctrl
Stim
order alternated
Time
c
Sham
Recording
Injection
TTX
Stim 1Hz
Ca2+ imaging
Amplitude (pA)
Before
After
Time
Time (s)
Control
Stimulation
Processes
Somata
d
Non-sheath
e
Sheath
h
Non-sheath
i
Sheath
0.1 ΔF/F
10 s
Stim.
f
Non-sheath
p=0.001
g
Sheath
p=0.002
j
Non-sheath
p=0.02
k
Sheath
p=0.28
Rate (per min)
Ctrl
Stim
l
Non-sheath
p=0.66
p=0.015
m
Sheath
p=0.42
p=0.001
Before
After
n
Non-sheath
p=0.72
p=0.026
o
Sheath
p=0.89
p=0.89
Sham
TTX

Fig. 2

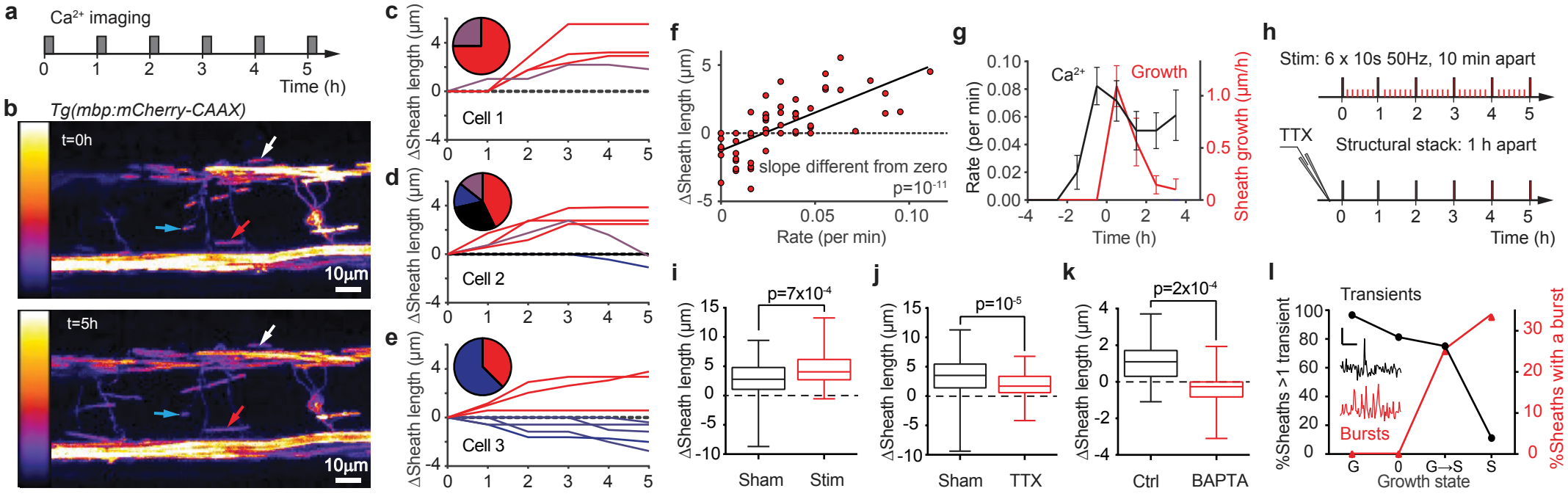
a
Ca2+ imaging
0 1 2 3 4 5
Time (h)
b
Tg(mbp:mCherry-CAAX)
t=0h
10µm
t=5h
10µm
c
ΔSheath length (µm)
Cell 1
d
Cell 2
e
Cell 3
f
slope different from zero
p=10-11
Rate (per min)
g
Ca2+
Growth
Rate (per min)
Sheath growth (µm/h)
Time (h)
h
Stim: 6 x 10s 50Hz, 10 min apart
TTX
Structural stack: 1 h apart
Time (h)
i
p=7x10-4
Sham
Stim
j
p=10-5
Sham
TTX
k
p=2x10-4
Ctrl
BAPTA
l
Transients
Bursts
%Sheaths >1 transient
%Sheaths with a burst
G
0
G→S
S
Growth state

Fig. 3

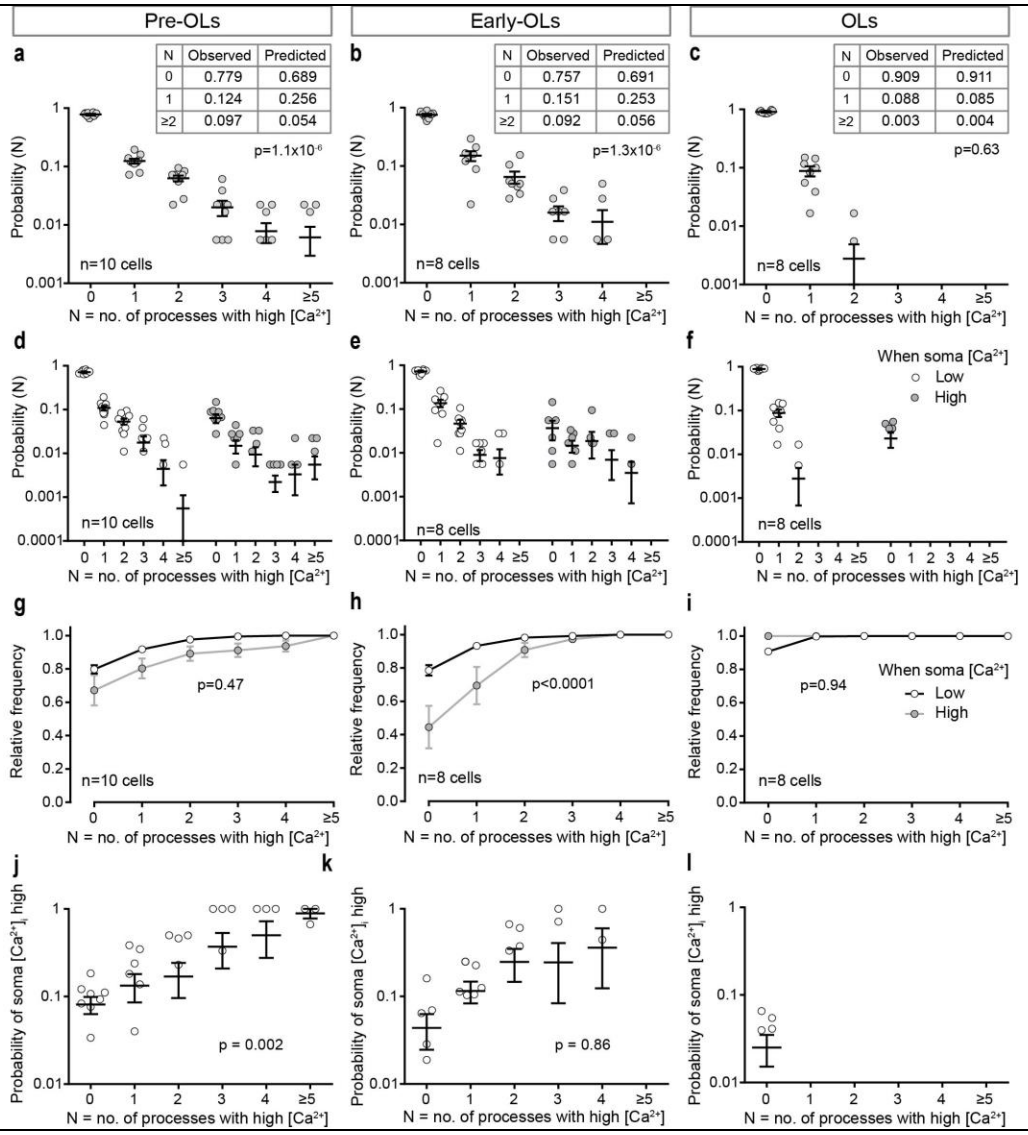

Supplementary Figure 1

Synchronicity of $[Ca^{2+}]_i$ transients in different cell regions.

(**a-c**) Charts: Fraction of time (Probability) that the number of processes on the abscissa (*N*) had a simultaneous $[Ca^{2+}]_i$ elevation, in (**a**) pre-OLs, (**b**) early-OLs and (**c**) OLs from 5, 6 and 6 animals respectively (mean values, shown as horizontal lines with SEM bars, that are below all visible individual data points reflect some data points being zero and hence not plotted on the logarithmic scale charts). Inset tables: Observed distribution of probability as in main graphs, and predicted distribution calculated as follows. If the probability of a single observed process having a high $[Ca^{2+}]_i$ is denoted p_1 (this was derived experimentally for each process and averaged over all the processes of each individual cell), and there are *N* processes, the probability of *k* processes exhibiting calcium transients simultaneously is: $p(k) = \frac{N! p_1^k (1-p_1)^{N-k}}{k!(N-k)!}$. These are the predicted values in the inset tables, when averaged over all cells. The observed values for the fraction of time that 2 or more processes simultaneously showed a high $[Ca^{2+}]_i$ were greater than predicted for pre-OLs and early-OLs, implying cooperativity of transient generation between processes or propagation of transients from one process into another, but not for OLs (see 2-sided Chi-squared p values for inset tables). (**d-f**) Probabilities of *N* (abscissa) processes having high $[Ca^{2+}]_i$ simultaneously and having the soma $[Ca^{2+}]_i$ low (black bars) or high (i.e. during a soma $[Ca^{2+}]_i$ transient, grey bars), for each of the 3 classes of cell. (**g-i**) Cumulative probability distributions for the data in d-f, with p values from Kolmogorov-Smirnov tests comparing the distributions for each cell class. When the soma $[Ca^{2+}]_i$ was high in early-OLs, there was a larger probability for 1 or more processes to have an elevated $[Ca^{2+}]_i$, than was the case when the soma $[Ca^{2+}]_i$ was low. Soma transients occurred with a probability of 0.10, 0.08 and 0.02 for pre-OLs, early-OLs and OLs, respectively, and so the majority of $[Ca^{2+}]_i$ transients in processes

occurred when soma $[Ca^{2+}]_i$ was low. In OLs in particular, processes only showed $[Ca^{2+}]_i$ elevations when the soma $[Ca^{2+}]_i$ was low, and the data in panel c imply that $[Ca^{2+}]_i$ transients in different myelin sheaths are independent of each other. (**j-l**) Probability of the soma $[Ca^{2+}]_i$ being high when the number of processes on the abscissa simultaneously exhibited high $[Ca^{2+}]_i$ for each of the 3 classes of cell. For pre-OLs the probability of the soma $[Ca^{2+}]_i$ being high is increased when more processes have a simultaneously high $[Ca^{2+}]_i$ ($p=0.0024$, ANOVA) indicating that gene expression might be controlled by somatic $[Ca^{2+}]_i$ elevations triggered by simultaneous activity-evoked transients in several processes on the same developing oligodendrocyte. For early-OLs the increase of probability with number of processes simultaneously exhibiting high $[Ca^{2+}]_i$ did not reach significance ($p=0.86$, Kruskal-Wallis test). For OLs, the soma $[Ca^{2+}]_i$ was never high when process $[Ca^{2+}]_i$ was high. All data are mean±SEM.

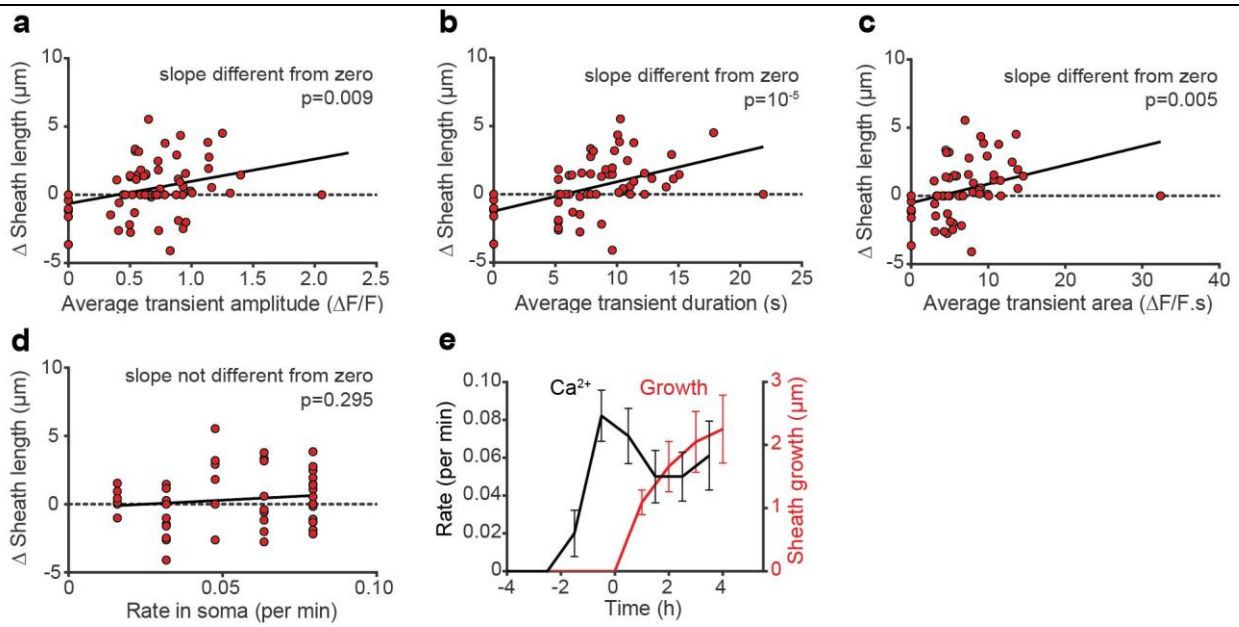

Supplementary Figure 2

Dependence of sheath elongation on $[Ca^{2+}]_i$ properties.

(**a-c**) Change of sheath length (in 68 sheaths from 6 animals) correlates significantly with sheath $[Ca^{2+}]_i$ transient (**a**) duration, (**b**) amplitude and (**c**) area (∫[ΔF/F] dt). (**d**) Change of sheath length does not correlate significantly with soma $[Ca^{2+}]_i$ transient rate (in 54 sheath-soma pairs from 6 animals). (**e**) Increase of sheath length and $[Ca^{2+}]_i$ transient rate in 14 lengthening sheaths which were of constant length for at least 1 hour before lengthening started, with data aligned at t=0 at the start of growth. $[Ca^{2+}]_i$ transients precede sheath growth by ~1 hour. Data are mean±SEM.